Supporting Information

$Ti_3C_2T_x$ MXene/Carbon Nanofiber Multifunction Electrode for Electrodeionization with Antifouling Activity

Jingjing Lei[1], Fei Yu[2], Haijiao Xie[3], Jie Ma[1*]

[1] Research Center for Environmental Functional Materials, State Key Laboratory of Pollution Control and Resource Reuse, College of Environmental Science and Engineering, Tongji University, 1239 Siping Road, Shanghai 200092, P.R. China

[2] College of Marine Ecology and Environment, Shanghai Ocean University, No 999, Huchenghuan Road, Shanghai, 201306, P.R. China

[3] Hangzhou Yanqu Information Technology Co., Ltd., Y2, 2 nd Floor, Building 2, Xixi Legu Creative Pioneering Park, 712 Wen'er West Road, Xihu District, Hangzhou, Zhejiang, 310003, P.R. China

*Corresponding authors: Jie Ma, E-mail: jma@tongji.edu.cn

Experimental section

Preparation of $Ti_3C_2T_x$ nanosheets

The $Ti_3C_2T_x$ nanosheets were prepared by selectively etching the Al layer from the Ti_3AlC_2 MAX phases precursor followed by the exfoliation, and the steps were as follows. 1 g of LiF was added to 20 mL hydrochloric acid (HCl, 9 mol L^{-1}) and stirred for 20 min. Then 1 g of Ti_3AlC_2 (11 Technology Co., Ltd., Jilin, China) was added and stirred at 40°C for 48 h. The obtained were washed with deionized water and centrifuged at 3500 rpm until the pH value reached greater than ~6. Ethanol (intercalator) was added to the obtained $Ti_3C_2T_x$ precipitate followed by ultrasonication in an ice bath for 1 h, and then the precipitate was collected by centrifugation at 10000 rpm for 10 min. Deionized water was added and ultrasonicated in an ice bath under Ar flow for 20 min and the supernatant (monolayer or few-layers $Ti_3C_2T_x$ nanosheets solution) was collected by centrifugation at 3500 rpm for 5 min. The ultrasonication and centrifugation operations were repeated many times to obtain as much supernatant as possible. Finally, the supernatant was freeze-dried to obtain the $Ti_3C_2T_x$ nanosheet powder.

Electrospinning of $Ti_3C_2T_x$/PAN nanofibers film

The $Ti_3C_2T_x$ nanosheets powder was dispersed in 5 mL of N, N-Dimethylformamide (DMF), and the concentrations were controlled to be 1 wt%, 3 wt%, 5 wt%, 10 wt%, and 14 wt%, respectively. Subsequently, the suspension was ultrasonic cell grinded for 20 min in an ice bath, and the operating mode was set to work for 2 s and intermittently for 3 s. Finally, 0.9 g of PAN (M_w=150000, Macklin Biochemical Technology Co., Ltd., Shanghai, China) was added, and the mixture was stirred at room temperature for more than 6 h.

The spinning solution prepared above was loaded into a 5mL syringe with a 21-gauge metal needle. The solution flow rate was maintained at 1.0 mL h^{-1}. The needle tip-collector distance was fixed to 18 cm. A high voltage of 18 kV was applied between the needle tip and the roller to produce fibers on the aluminum foil around the roller, which was rotated at a speed of 60 rpm. The temperature and humidity of the spinning environment were maintained at 25°C and 35%, respectively. The as-spun fiber films with different concentrations of $Ti_3C_2T_x$ were named as $Ti_3C_2T_x$/PAN-1, $Ti_3C_2T_x$/PAN-3, $Ti_3C_2T_x$/PAN-5, $Ti_3C_2T_x$/PAN-10, $Ti_3C_2T_x$/PAN-14,

respectively.

Fabrication of the $Ti_3C_2T_x$/CNF film

The as-spun fiber films were stabilized and carbonized by a gradient heating strategy. The samples were first heated in air from room temperature to 200 °C at a rate of 5 °C min^{-1}, followed by heated to 250 °C at a rate of 1 °C min^{-1} and stabilized for 1 h. Then, the temperature was raised to 800°C at a rate of 5°C min^{-1} under an Ar atmosphere and carbonized for 2 h to obtain the self-supporting $Ti_3C_2T_x$/CNF film.

Characterization techniques

The morphology and structure of the samples were examined with the scanning electron microscope (SEM, Hitachi S-4800, Japan) and transmission electron microscopy (TEM, JEM-2100F, Japan). The compositions of the samples were analyzed by energy-dispersive X-ray spectroscope (EDX) attached to the SEM instrument. The crystalline phases of the samples were affirmed by Powder X-ray diffraction (XRD, Bruker D8 Advance, Germany). Raman spectrum was collected through a Raman spectrometer (Horiba, Japan) to study the vibration modes and lattice behaviors of the samples. The Fourier transform infrared (FTIR) was conducted by using a Bruker Vertex 70 FTIR spectrometer. The surface chemical states of the samples were examined by a Thermo Scientific X-ray Photoelectron Spectroscopy system (XPS) with an Al Kα radiation source. Thermogravimetric analysis (TGA) was carried out in N_2 atmosphere with a ramping rate of 10 °C min^{-1}.

Electrochemical tests

The electrochemical tests including cyclic voltammetry (CV), galvanostatic charge/discharge (GCD), and electrochemical impedance spectroscopy (EIS) measurements were conducted using an electrochemical workstation (CHI660D, Shanghai Chenhua Instruments Co.) with a three-electrode system in 1 mol L^{-1} NaCl solution, with Pt electrode and Ag/AgCl as the counter electrode and reference electrode, respectively. The working electrode was obtained by directly cutting the fiber film sample into small pieces of 1×1 cm^2 and sticking it on graphite paper with conductive tape. The CV and GCD measurements were carried out in the potential range of -0.2 V to 0.6 V, while the EIS measurement was in the frequency range from 0.01 Hz to 100 kHz. The specific capacitance C (F g^{-1}) was calculated by the

following formula,

$$C = \frac{\int IdV}{2v\Delta Vm} \quad (1)$$

where ΔV is the potential window (V), I is the response current (A), m is the mass of active material (g), and v is the scan rate (V s^{-1}).

Desalination measurements

The batch mode configuration was employed in the desalination measurements, in which 40 mL of NaCl solution was pumped through the CDI cell and circulated at a flow rate of 20 mL min^{-1} using a peristaltic pump. The desalination experiments were performed in a constant current mode, with different initial NaCl concentrations (5 mM, 10 mM, 20 mM, 40 mM, and 80 mM), current densities (60 mA g^{-1}, 70 mA g^{-1}, 80 mA g^{-1} and 100 mA g^{-1}), and cut-off voltages (0.6 V, 0.8 V, 1.0 V, 1.2 V and 1.4 V) set by the battery test system (Wuhan Landian Electronics Co., Ltd., 8002A).

The real-time conductivity of the NaCl solution was monitored and recorded using a conductivity meter (Mettler Toledo S230).

The desalination capacity (DC, mg·g^{-1}) was computed based on the following equation,

$$DC = \frac{(C_0 - C_e) \times V}{m} \quad (2)$$

where C_0 and C_e are the initial and balanced concentration (mg·L^{-1}) of the NaCl solution calculated according to the conductivity, respectively, V is the volume (L) of the NaCl solution, and m is the total mass (g) of the electrode including the cathode and anode.

The average desalination rate (ADR, mg·g^{-1}·min^{-1}) was calculated based on the following equation,

$$ADR = \frac{DC}{t} \quad (3)$$

where t is the desalination time (min).

The charge efficiency (Λ, %) and energy consumption (E, kWh kg^{-1}) are defined as follows:

$$\Lambda = \frac{F \times (C_0 - C_e) \times V}{M \times I \times t} \quad (4)$$

$$E = \frac{I \times \int v dt}{3600 \times (C_0 - C_e) \times V} \quad (5)$$

where F is the Faraday constant (96485 C mol^{-1}), M is the molar mass of NaCl (58.44g mol^{-1}), I is the current (A), and v is the voltage (V).

Bacterial culture and determination of antibacterial activity

The common and harmful Gram-negative *E. coli* was used as the target bacteria to evaluate the antibacterial activity of the samples. All materials and samples used in the experiment in contact with bacteria were sterilized by autoclaving at 121℃ for 20 min. The *E. coli* suspension was prepared as follows. The single colony of *E. coli* from the Nutrient Agar medium (NA) was picked and transferred to 100 mL Nutrient Broth medium (NB), and incubated overnight at 170 rpm and 37 ℃. 10 mL NB with *E. coli* in it was centrifuged at 5000 rpm for 10 min to collect bacteria, and then washed twice with sterile physiological saline water (NaCl, 0.85%) by centrifugation for the same speed and duration. After removal of the supernatant, the *E. coli* were resuspended in sterile physiological saline water and diluted to obtain *E. coli* suspension with a concentration of around 4.5×10^6 CFU/mL (CFU=colony forming units).

The antibacterial activity of the samples was determined by the plate-counting method. The prepared *E. coli* suspension (20 mL) and the samples (20 mg) were mixed and thoroughly contacted, respectively, and cultured with shaking at 170 rpm and 37 °C. The *E. coli* suspension was sampled and diluted at specific folds in sterile physiological saline water at each specific time interval (10min, 30min, 1h, 2h, and 4h). 100 μL dilutions were spread on the NA plates. All the plates were incubated for 24 h at 37 ℃ and 65% RH, and the number of colonies was counted. Control experiments were performed in parallel without any film samples. All the experiments were performed in triplicate. The inactivation efficiency (R) of the film samples against *E. coli* was calculated according to the following formula:

$$R = \frac{N_0 - N_t}{N_0} \times 100\% \quad (6)$$

where N_0 is the bacterial concentration of the blank control culture at time t, and N_t is

the bacterial concentration at time *t*. The bacterial concentration (CFU/mL) was obtained by multiplying the number of colonies by the dilution factor.

The kinetics of bacterial inactivation is described by the pseudo-first-order kinetic equation, Chick's classical disinfection model, whereby the logarithmic inactivation of bacteria is linearly related to treatment time:

$$log\frac{N_t}{N_0} = -kt \tag{7}$$

where *t* is the treatment time (min), and *k* is the kinetic constant for inactivation (min^{-1}).

Theoretical calculation method

The density functional theory (DFT) calculations[1, 2] were performed in the Vienna *ab initio* simulation package (VASP) based on the plane-wave basis sets with the projector augmented-wave method[3, 4]. The exchange-correlation potential was processed by a generalized gradient approximation (GGA) with the Perdew-Burke-Ernzerhof (PBE) parametrization[5]. The van der Waals correction of Grimme's DFT-D3 model was also adopted[6]. The supercell of graphene, Ti-C, and graphene/Ti-C interface model was used to model adsorption system (Na and Cl). As calculating the adsorption energy, the energies of the Cl and Na atoms in the bulk phase were used as a reference for total energy. The cut-off energy was set to 520 eV. The Brillouin-zone integration was sampled with a Γ-centered Monkhorst-Pack mesh[7] of 1 × 1 × 1. The structures were completely relaxed until the maximum force on each atom was less than 0.01 eV/Å, and the energy convergent standard was 10^{-5} eV.

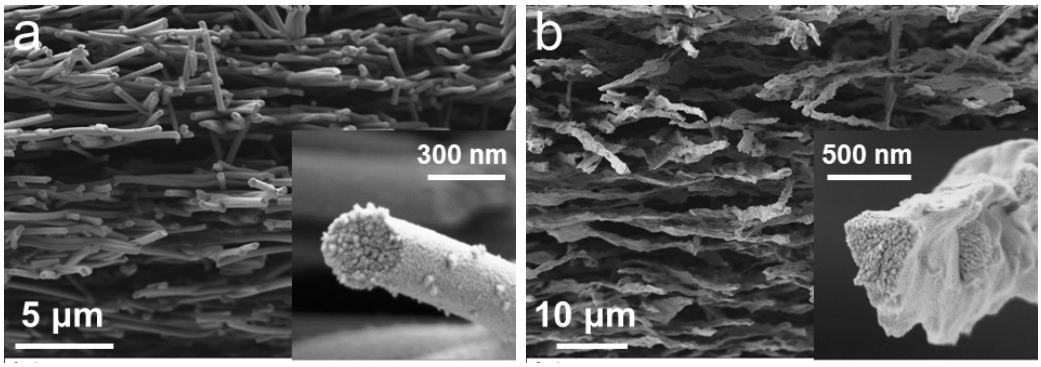

Figure S1. SEM images of the cross section of PAN nanofiber film (a) and $Ti_3C_2T_x$/PAN-14 (b).

Figure S2. Optical images of CNF.

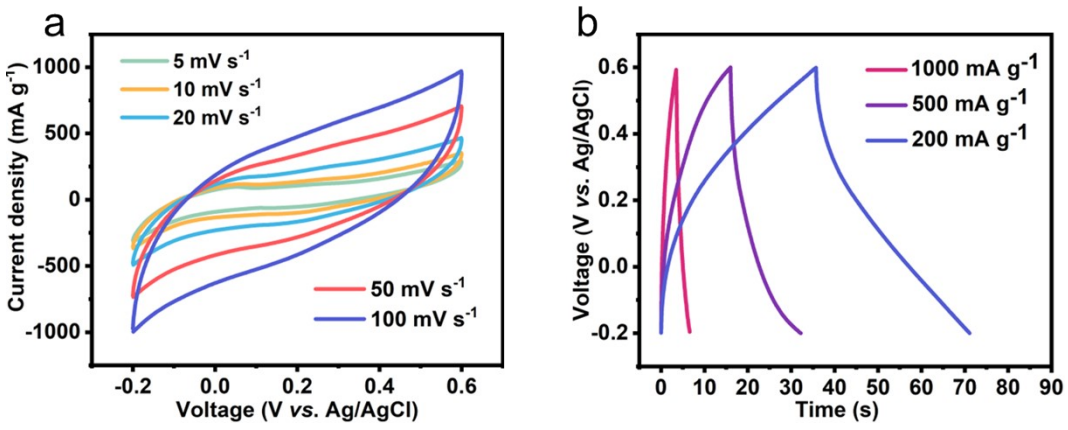

Figure S3. CV curves at different scan rates (a) and GCD profiles at different current densities (b) of CNF.

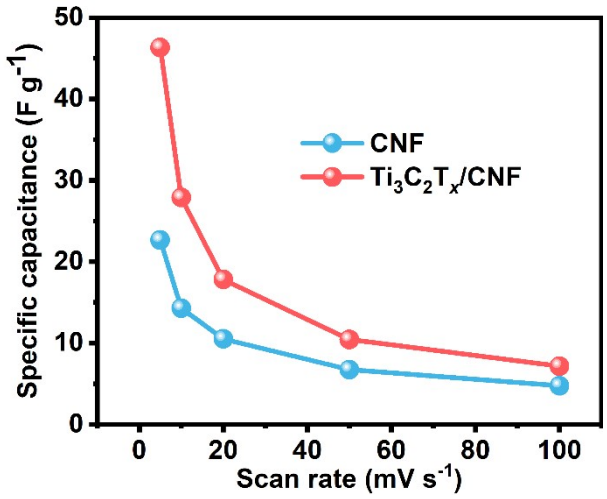

Figure S4. Specific capacitances of CNF and $Ti_3C_2T_x$/CNF-14.

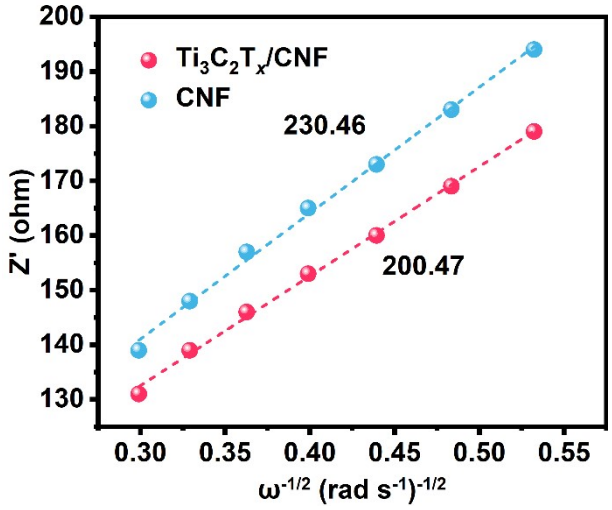

Figure S5. Plots of the relationship between Z' and $\omega^{-1/2}$ in the low-frequency region.

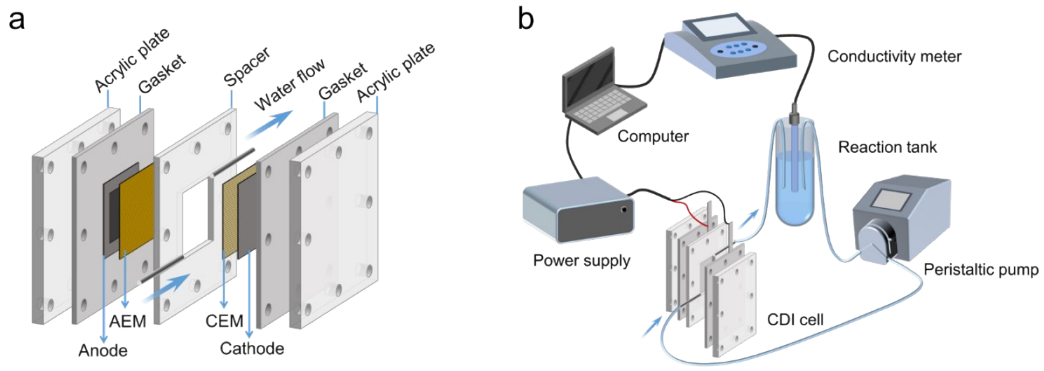

Figure S6. Schematic diagram of the CDI cell (a) and the bach mode of desalination system (b).

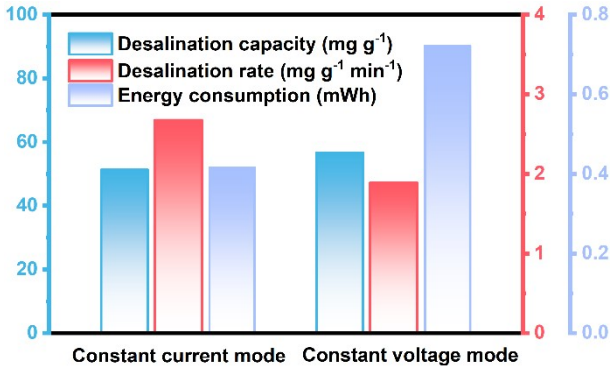

Figure S7. CDI performance comparison of constant current mode and constant voltage mode

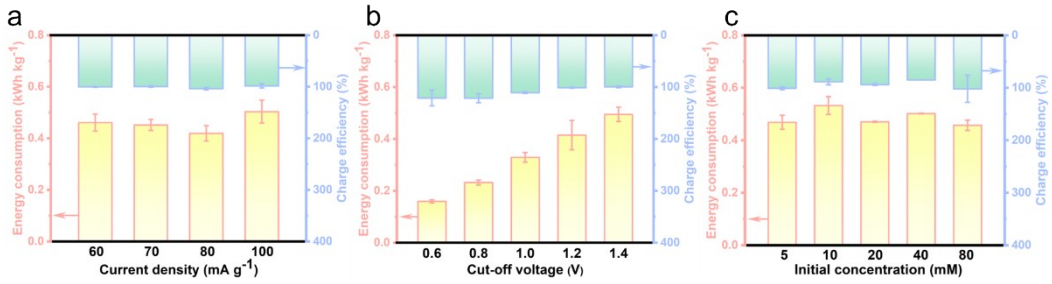

Figure S8. The energy consumption and charge efficiency of $Ti_3C_2T_x$/CNF-14 at different current densities (a), cut-off voltages (b), and NaCl initial concentration (c).

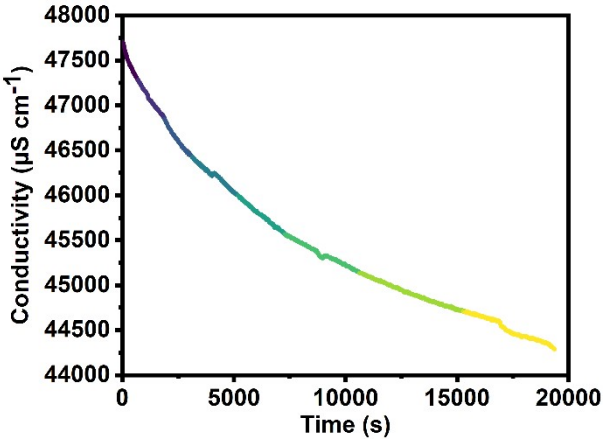

Figure S9. The conductivity changes of $Ti_3C_2T_x$/CNF-14 electrode in 600mM NaCl aqueous solution at 1.4 V.

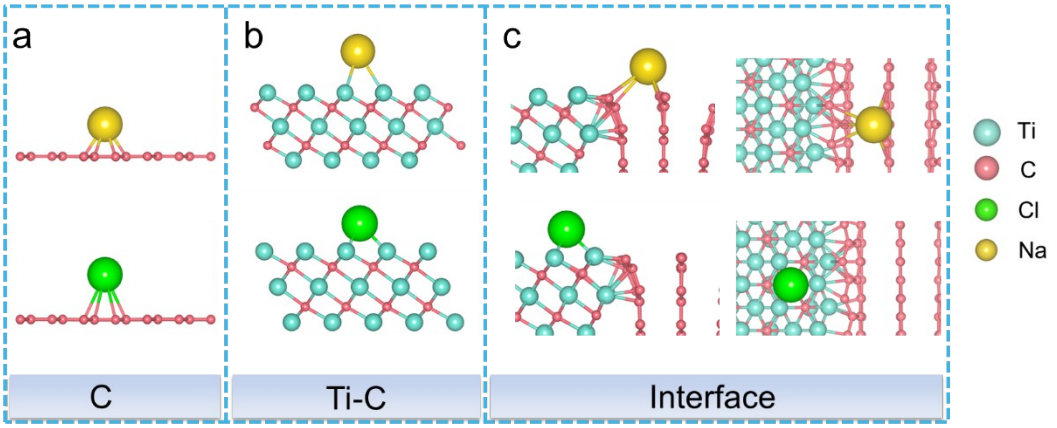

Figure S10. The optimized structures of Na and Cl adsorbed by CNF (a), $Ti_3C_2T_x$ (b) and $Ti_3C_2T_x$/CNF (c).

Table S1. The $Ti_3C_2T_x$ concentration and content of samples.

Samples	$Ti_3C_2T_x$ concentration in electrospinning solution	$Ti_3C_2T_x$ content in carbon nanofiber films
$Ti_3C_2T_x$/PAN-1	1 wt%	6.10 wt%
$Ti_3C_2T_x$/PAN-3	3 wt%	8.06 wt%
$Ti_3C_2T_x$/PAN-5	5 wt%	10.70 wt%
$Ti_3C_2T_x$/PAN-10	10 wt%	15.75 wt%
$Ti_3C_2T_x$/PAN-14	14 wt%	23.09 wt%

Table S2. The values of k and R^2 fitted according to Chick model.

Sample	$Ti_3C_2T_x$/CNF-1	$Ti_3C_2T_x$/CNF-3	$Ti_3C_2T_x$/CNF-5	$Ti_3C_2T_x$/CNF-10	$Ti_3C_2T_x$/CNF-14
k (min^{-1})	0.00182	0.00341	0.00465	0.00911	0.01303
R^2	0.996	0.991	0.991	0.982	0.977

Table S3. The circulating water parameters of Sinopec Engineering Group Luoyang R&D Center of Technologies

parameter	value
pH	7.02
Alkalinity (mg/L)	206
Ammonia nitrogen (mg/L)	0.83
COD (mg/L)	98
Fe^{3+} (mg/L)	1.9
Al^{3+} (mg/L)	0
K^{+} (mg/L)	30.28
Si (mg/L)	19.25
Ca^{2+} (mg/L)	270
Mg^{2+} (mg/L)	138
Cl^{-} (mg/L)	711
SO_4^{2-} (mg/L)	1430

Table S4. The performance comparison of $Ti_3C_2T_x$/CNF-14 with other reported electrodes.

Electrode materials	Self-supporting or not	Initial salt concentration (mg L^{-1})	Applied voltage/ Current density	Desalination capacity (mg g^{-1})	Average desalination rate (mg g^{-1} min^{-1})	Ref.
Commercial activated carbon	No	292.5	1.2 V	13.1	0.437	[8]
Commercial activated carbon cloth	Yes	292.5	1.2 V	16	0.53	[9]
Porous carbon nanosheets	No	500	1.1 V	15.6	1.56	[10]
Carbon spheres	No	500	1.2 V	15.8	0.35	[11]
N-doped carbon nanorods	No	500	1.2 V	17.62	0.44	[12]
N-doped mesostructured carbon	No	584	1.2 V	20.63	0.69	[13]
N-doped mesoporous carbon	No	250	1.6 V	26.20	0.44	[14]
Polyaniline activated carbon	No	600	1.2 V	22.2	1.11	[15]
Activated biochar	No	292.5	1.2 V	28.9	0.48	[16]
Porous carbon fibers	Yes	500	1.0 V	30	3.0	[17]
N, P-doped carbon–graphene	No	1000	1.2 V	39.34	1.31	[18]
HF - Ti_3C_2	No	292.5	1.2 V	13	1	[19]
porous $Ti_3C_2T_x$	No	10000	1.2 V	45	2.81	[20]
N-$Ti_3C_2T_x$	No	5000	1.2 V	43.5	3.71	[21]
NaOH-$Ti_3C_2T_x$	No	500	1.2 V	16.02	1.07	[22]
LiF / HCl - $Ti_3C_2T_x$	Yes	585	1.2 V 20 mA g^{-1}	67.7	0.81	[23]
L−S-$Ti_3C_2T_x$	Yes	585	1.6V 30 mA g^{-1}	72	1.66	[24]

Alk-$Ti_3C_2T_x$-M	Yes	1000	1.2V 30 mA g^{-1}	50	1.63	[25]
CLF@ $Ti_3C_2T_x$	No	600	1.2 V	34	0.56	[26]
PPy-NiCo-LDH@Mxene	No	500	1.2 V	31.5	1.89	[27]
MoS_2/MXene	No	500	1.2 V	23.98	0.8	[28]
MoS_2@MXene	No	500	1.2 V	35.6	1.07	[29]
MXene@COF	No	500	1.2 V	24.5	0.82	[30]
$Ti_3C_2T_x$/CNF	**Yes**	**585**	**1.2 V** **60 mA g^{-1}**	**73.42**	**2.19**	**This work**

References

1. Hohenberg, P. and W. Kohn, *Inhomogeneous Electron Gas.* Physical Review, 1964. **136**(3B): p. B864-B871.
2. Kohn, W. and L.J. Sham, *Self-Consistent Equations Including Exchange and Correlation Effects.* Physical Review, 1965. **140**(4A): p. A1133-A1138.
3. Kresse, G. and J. Furthmüller, *Efficient iterative schemes for ab initio total-energy calculations using a plane-wave basis set.* Physical review B, 1996. **54**(16): p. 11169.
4. Blöchl, P.E., *Projector augmented-wave method.* Physical Review B, 1994. **50**(24): p. 17953-17979.
5. Perdew, J.P., K. Burke, and M. Ernzerhof, *Generalized gradient approximation made simple.* Physical Review Letters, 1996. **77**(18): p. 3865.
6. Grimme, S., et al., *A consistent and accurate ab initio parametrization of density functional dispersion correction (DFT-D) for the 94 elements H-Pu.* The Journal of Chemical Physics, 2010. **132**(15): p. 154104.
7. Monkhorst, H.J. and J.D. Pack, *Special points for Brillouin-zone integrations.* Physical Review B, 1976.
8. Aslan, M., et al., *Improved capacitive deionization performance of mixed hydrophobic/hydrophilic activated carbon electrodes.* J Phys Condens Matter, 2016. **28**(11): p. 114003.
9. Kim, C., et al., *Influence of pore structure and cell voltage of activated carbon cloth as a versatile electrode material for capacitive deionization.* Carbon, 2017. **122**: p. 329-335.
10. Wu, T., et al., *Starch Derived Porous Carbon Nanosheets for High-Performance Photovoltaic Capacitive Deionization.* Environ Sci Technol, 2017. **51**(16): p. 9244-9251.
11. Xu, X., et al., *Carbon spheres with hierarchical micro/mesopores for water desalination by capacitive deionization.* Journal of Materials Chemistry A, 2016. **4**(41): p. 16094-16100.
12. Liu, Y., et al., *Nitrogen-doped carbon nanorods with excellent capacitive deionization ability.* Journal of Materials Chemistry A, 2015. **3**(33): p. 17304-17311.
13. Xu, X., et al., *Capacitive deionization using nitrogen-doped mesostructured carbons for highly efficient brackish water desalination.* Chemical Engineering Journal, 2019. **362**: p. 887-896.
14. Tian, S., et al., *Capacitive deionization with nitrogen-doped highly ordered mesoporous carbon electrodes.* Chemical Engineering Journal, 2020. **380**: p. 122514.
15. Zornitta, R.L., et al., *Understanding the mechanism of carbonization and KOH activation of polyaniline leading to enhanced electrosorption performance.* Carbon, 2020. **156**: p. 346-358.
16. Tang, Y.H., S.H. Liu, and D.C.W. Tsang, *Microwave-assisted production of CO2-activated biochar from sugarcane bagasse for electrochemical desalination.* J Hazard Mater, 2020. **383**: p. 121192.
17. Liu, T.Y., et al., *Exceptional capacitive deionization rate and capacity by block copolymer-based porous carbon fibers.* SCIENCE ADVANCES, 2020. **6**(16).
18. Guo, J., et al., *Graphene-carbon 2D heterostructures with hierarchically-porous P,N-doped layered architecture for capacitive deionization.* Chem Sci, 2021. **12**(30): p. 10334-10340.
19. Srimuk, P., et al., *MXene as a novel intercalation-type pseudocapacitive cathode and anode for capacitive deionization.* Journal of Materials Chemistry A, 2016. **4**(47): p. 18265-18271.
20. Bao, W., et al., *Porous Cryo-Dried MXene for Efficient Capacitive Deionization.* Joule, 2018.

2(4): p. 778-787.
21. Amiri, A., et al., *Porous nitrogen-doped MXene-based electrodes for capacitive deionization.* Energy Storage Materials, 2020. **25**: p. 731-739.
22. Chen, B., et al., *MXene as a Cation-Selective Cathode Material for Asymmetric Capacitive Deionization.* ACS Appl Mater Interfaces, 2020. **12**(12): p. 13750-13758.
23. Ma, J., et al., *Free-standing Ti3C2Tx MXene film as binder-free electrode in capacitive deionization with an ultrahigh desalination capacity.* Chemical Engineering Journal, 2020. **384**.
24. Shen, X., et al., *All-MXene-Based Integrated Membrane Electrode Constructed using Ti3C2Tx as an Intercalating Agent for High-Performance Desalination.* Environ Sci Technol, 2020. **54**(7): p. 4554-4563.
25. Shen, X., et al., *Free-standing 3D alkalized Ti3C2Tx/Ti3C2Tx nanosheet membrane electrode for highly efficient and stable desalination in hybrid capacitive deionization.* Journal of Materials Chemistry A, 2020. **8**(37): p. 19309-19318.
26. Anwer, S., et al., *2D Ti3C2Tx MXene nanosheets coated cellulose fibers based 3D nanostructures for efficient water desalination.* Chemical Engineering Journal, 2021. **406**.
27. Cai, Y., et al., *Flexible structural engineering of PPy-NiCo-LDH@Mxene for improved capacitive deionization and efficient hard water softening process.* Separation and Purification Technology, 2022. **280**.
28. Chen, Z., et al., *Ultra-durable and highly-efficient hybrid capacitive deionization by MXene confined MoS2 heterostructure.* Desalination, 2022. **528**.
29. Cai, Y., et al., *3D Heterostructure Constructed by Few-Layered MXenes with a MoS2 Layer as the Shielding Shell for Excellent Hybrid Capacitive Deionization and Enhanced Structural Stability.* ACS Appl Mater Interfaces, 2022. **14**(2): p. 2833-2847.
30. Zhang, S., et al., *Heterointerface optimization in a covalent organic framework-on-MXene for high-performance capacitive deionization of oxygenated saline water.* Mater Horiz, 2022. **9**(6): p. 1708-1716.